Research Article

Nano Research
2022, 15(3): 2746–2755

ISSN 1998-0124 CN 11-5974/O4
https://doi.org/10.1007/s12274-021-3847-4

Hierarchical utilization of raw $Ti_3C_2T_x$ MXene for fast preparation of various $Ti_3C_2T_x$ MXene derivatives

Shunlong Zhang[§], Hangjun Ying[§], Pengfei Huang, Tiantian Yang, and Wei-Qiang Han (✉)

School of Materials Science and Engineering, Zhejiang University, Hangzhou 310027, China
[§] Shunlong Zhang and Hangjun Ying contributed equally to this work.

Received: 9 June 2021 / **Revised:** 26 July 2021 / **Accepted:** 27 August 2021

ABSTRACT

Due to easy re-stacking, low yield of few-layered MXenes (f-MXenes), the applications of MXenes are mainly restricted in multi-layered MXenes (m-MXenes) state. Although f-MXenes can be prepared from m-MXenes, after exfoliation process, a mass of sediments which are still essentially compact MXenes are usually directly discarded, leading to low utilization of raw m-MXenes. Herein, a classified preparation strategy is adopted to exploit the raw m-MXenes and traditional MXenes sediments, taking multi-layered $Ti_3C_2T_x$ MXene as an example. Via rational delamination and subsequent treatment to $Ti_3C_2T_x$ sediments, we succeed in achieving classified and large-scale preparation of various $Ti_3C_2T_x$ MXene derivatives, including few-layered $Ti_3C_2T_x$ (f-$Ti_3C_2T_x$) powders, f-$Ti_3C_2T_x$ films, and $Ti_3C_2T_x$ MXene-derived nanowires with heterostructure of potassium titanate and $Ti_3C_2T_x$. We demonstrate the necessity of "step-by-step delamination" towards traditional $Ti_3C_2T_x$ sediments to improve the yield of f-$Ti_3C_2T_x$ from 15% to 72%; the feasibility of "solution-phase flocculation (SPF)" to fundamentally solve the re-stacking phenomenon, and oxidation degradation issues of f-$Ti_3C_2T_x$ during storage; as well as the convenience of SPF to deal with time-consuming issues of fabricating $Ti_3C_2T_x$ films. What's more, alkali-heat treatment of final $Ti_3C_2T_x$ sediments turns waste into treasure of $Ti_3C_2T_x$-derived nanowires, leading to 100% utilization of raw $Ti_3C_2T_x$. The content of one-dimensional (1D) nanowires in the hybrids can be adjusted by controlling alkalization time. The 3D architecture heterostructure composed of 1D nanowires and 2D nanosheets exhibits gorgeous application potential. This work can expand preparation and application of various MXenes derivatives, promoting process of various MXenes.

KEYWORDS

MXenes, MXenes derivatives, $Ti_3C_2T_x$, step-by-step delamination, solution-phase flocculation, Alkali-heat treatment

1 Introduction

As an emerging family of two-dimensional materials, transition metal carbonitrides, derived from MAX phase [1–3], MXenes have accumulated tremendous interests [4–6]. The generic formula of MXenes can be denoted as $M_{n+1}X_nT_x$, where M, X, and T_x represent transition metals, C, and/or N, terminated functional groups of –O, –OH, –F, etc. respectively [7, 8]. A lot of researches have proved that MXenes display excellent figures of merit in various fields, involving energy storage [9, 10], catalysis [11, 12], electromagnetic shielding [13–15], and so on (Fig. S1 in the Electronic Supplementary Material (ESM)) [16, 17]. In particular, the variety in composition, the rich surface chemistry, and large interlayer spacing of MXenes make MXenes distinguished among two-dimensional (2D) materials [18]. Since discovered in 2011, many works closely focus on the study of fundamental preparation-structure-function correlation, which is highly significant to the development of MXenes [19–22]. Among MXenes family [23, 24], $Ti_3C_2T_x$, usually prepared from Ti_3AlC_2 MAX with various etching methods, has been intensively studied due to its merits of ultra-high conductivity (~ 15,000 S/cm), excellent mechanical strength, and good energy storage characteristics [25–27].

It is well known that the number of layers of 2D materials has great impact on its fundamental properties, and further affects its final functional performance. The thinner the 2D materials, the better the final functional performance. Therefore, the preparation and application of few-layered or single-layered MXenes (f-MXenes, s-MXenes) is a research hotspot. However, f-MXenes and s-MXenes are faced with problems of easy re-stacking [28], together with low yield about 15% and large amount of sediments wastes [29, 30]. As result, a considerable part of the reports about MXenes were blocked at multi-layered MXenes (m-MXenes) state [31]. In recent years, there have been some reports about f-MXenes, which suppress re-stacking phenomenon with assistance of additional components, such as carbon nanotube (CNT), graphene [32]. However, the introduction of the extra components makes it confusing to judge which component works in the composites [18]. Hence, it is significant to fast prepare f-MXenes or even s-MXenes with high yield.

To date, there are still some basic problems to be solved, including the following challenges: (1) The yields of f-MXenes (10%–15%) through delamination of m-MXenes are far from satisfactory. The residues (up to 85% or even higher) are directly discarded in most previous reports [29], which results in low utilization of raw MXenes and high price, as well as failure of large-

Address correspondence to hanwq@zju.edu.cn

scale preparation. It's an urgent need to improve delamination yield of f-MXenes and exploit applications of the sediments waste. (2) In order to avoid re-stacking, delaminated MXenes are usually dispersed in water due to hydrophilicity. However, it is accompanied with inevitable degradation because of interaction between water molecule and the surface groups of MXenes, even under protection of Ar atmosphere, low-temperature environment, or polyanion antioxidants [33]. Moreover, these approaches are high energy consumption or need subsequent process to remove additives. Fast preparation of delaminated MXenes into powders state, which can be stored in a water and oxygen free environment, is a radical solution to the degradation and oxidation problems. However, it is still faced with great challenge to quickly prepare f-MXenes powders via freeze-drying process because of the easy re-stacking problems, together with excessive content of dispersant water. (3) MXenes films have been used in various applications [34, 35]. However, the general vacuum filtration of MXenes films is quite time-consuming due to re-stacking of delaminated MXenes nanosheets under vacuum force. It takes 5–10 h to filter per film with thickness about 30 μm. Therefore, how to improve the preparing efficiency of flexible MXenes films is also of big challenge [34–36].

As a result, we can put forward the following meaningful questions: (1) How to completely solve the oxidation problem of MXenes during storage in a simple way? (2) How to improve the delamination efficiency of m-MXenes and the yield of f-MXenes or even s-MXenes nanosheets? (3) How to realize fast preparation of f-MXenes or s-MXenes nanosheets powders and self-supporting MXenes films? (4) How to rationally use the sediments residues after collecting the supernatant, rather than directly discard them? These fundamental issues are the main bottlenecks and of great significance for the in-depth development of MXenes family. Therefore, the new guidelines for systematic preparation of MXenes-derived materials by simple and scalable process are highly desired.

Aimed at the above problems, we propose the guidelines of classified preparation, involving key points of step-by-step delamination (SBSD) strategy, modified solution-phase flocculation (MSPF) method, and alkali-heat treatment (AHT) toward final MXenes sediments. Remarkably, we achieve in fast preparation of f-$Ti_3C_2T_x$ nanosheets powders with yield of 72%, self-supporting flexible f-$Ti_3C_2T_x$ films within ~ 5 min. All the samples can be stored in dry inert environment, leading to thorough avoid of oxidation degradation of MXenes. Besides, 100% utilization of MXenes sediments and raw m-MXenes can be achieved by transforming the final MXenes sediments residues into useful MXenes-derived nanowires, which can be various alkali metal titanate, depending on the condition of AHT process. According to published literatures [37, 38], MXenes derivatives prepared in this paper have broad application prospects, which are determined by their superior microstructure and fundamental properties. Furthermore, products in this paper can be prepared on a large scale based on the simple preparation methods. More importantly, in this work, we mainly focus on the MXenes sediments wastes, which are usually directly discarded after ultrasonic exfoliation process. Alkali-heat treatment can turn trash of MXenes sediments into treasure of MXenes-derived nanowires.

2 Experimental sections

Classified preparation and hierarchical 100% utilization of raw MXenes, taking $Ti_3C_2T_x$ MXene as an example.

2.1 Preparation of m-$Ti_3C_2T_x$ MXenes powders

Gray Ti_3AlC_2 powders (98%, 200 mesh) were purchased from Beijing Forsman Technology Company. The accordion-like m-$Ti_3C_2T_x$ powders were prepared according to previous reported hydrofluoric acid (HF) etching methods [39, 40].

2.2 Preparation of f-$Ti_3C_2T_x$ or s-$Ti_3C_2T_x$ MXenes powders, $Ti_3C_2T_x$ films

2.2.1 *Step-by-step delamination strategy*

In order to avoid formation of fragments and increase yields of delaminated MXenes nanosheets, SBSD strategy was proposed, which means the traditional sediments can be continuously delaminated after collection of supernatants (Fig. S2 in the ESM), until supernatant becomes nearly transparent. In detail, 1 g accordion-like m-$Ti_3C_2T_x$ was immersed in 10 mL tetramethylammonium hydroxide (TMAOH, 25% water solution) with continuous stirring for 24 h. Then, the $Ti_3C_2T_x$ solution was centrifugated and washed with deionized (DI) water. Before ultrasonic treatment, the $Ti_3C_2T_x$ was soaked in DI water for 24 h. After ultrasonic treatment for 1 h, the delaminated $Ti_3C_2T_x$ supernatant can be collected via centrifugation (3,500 rpm, 30 min) according to previous research experience [39, 41]. The initial $Ti_3C_2T_x$ MXenes sediments can be further delaminated by SBSD strategy until nearly transparent supernatant, keeping the same process as the first time, including ultrasonic treatment and centrifugation collection.

2.2.2 *Solution-phase flocculation (SPF) method*

5 mL 1 M ammonium salts such as NH_4HCO_3 were added into 100 mL delaminated MXenes solution with continuous stirring. After resting for 24 h at refrigeration (5 °C), there was an obvious flocculation phenomenon. Most of the water can be removed at flocculation process. The fast preparation of $Ti_3C_2T_x$ powders via freeze-drying and $Ti_3C_2T_x$ films via vacuum-assisted filtration can be achieved, followed by subsequent annealing (Ar, 6 h, 120 °C) to remove ammonium ion based on the decomposition temperature of NH_4HCO_3 (60 °C). Similar flocculation phenomenon can also be observed if ammonium salts were replaced by hydrochloric acid, proving the feasibility of ammonium salts or hydrochloric acid in playing the role of flocculants. The proposed MSPF method can further accelerate the process of flocculation and remove water with assistance of appropriate low speed centrifugation (2,000 rpm, 5 min).

2.3 Preparation of $Ti_3C_2T_x$ MXenes sediments derived nanowires

After several times exfoliation, the final tile-like sediments intrinsically belong to m-$Ti_3C_2T_x$ that cannot be further easily delaminated. These sediments are usually directly discarded. In order to achieve 100% utilization of accordion-like raw m-$Ti_3C_2T_x$, the 0.5 g tile-like $Ti_3C_2T_x$ MXenes sediments were alkalized in 5 M 50 mL KOH aqueous solution with AHT at 50 °C for 6 days, marked as KTO-6. To study the transformation process, a series of $Ti_3C_2T_x$ sediments derived nanowires were prepared by adjusting alkalization time, such as KTO-2 (alkalization for 2 days), KTO-0 (fresh MXenes sediments). The content of 1D nanowires in the hybrids can be adjusted by controlling alkalization time.

2.4 Materials characterization

X-ray diffraction (XRD) measurements were carried out by Rigaku MiniFlex 600 (Cu Kα radiation). X-ray photoelectron spectroscopy (XPS) measurements were analyzed by Thermo Fisher 250XI. The morphology and microstructure of MXenes derivates, including powders, films, and nanowires, were characterized by scanning electron microscopy (SEM, Hitachi SU-

8010) and transmission electron microscopy (TEM, JEM-2100). Brunauer–Emmett–Teller (BET) surface area and N_2 adsorption–desorption isotherm curve were employed by Micromeritics ASAP 2020 Plus HD88.

2.5 Abbreviations

In this paper and associated supporting information, multi-layered is abbreviated as m-; few-layered is abbreviated as f-; single-layered is abbreviated as s-; step-by-step delamination is abbreviated as SBSD; solution-phase flocculation is abbreviated as SPF; modified solution-phase flocculation is abbreviated as MSPF; alkali-heat treatment is abbreviated as AHT, and reaction time of day is abbreviated as d.

3 Results and discussion

The overall preparation processes of delaminated MXenes powders, flexible films, and MXenes-derived nanowires are provided in Fig. 1 and Fig. S2 in the ESM, taking $Ti_3C_2T_x$ MXene as an example. After etching and pre-intercalated by various agents such as tetramethylammonium hydroxide (TMAOH), the accordion-like m-MXenes can be exfoliated into f-MXenes or even s-MXenes. In order to improve delamination efficiency and avoid formation of MXenes fragments owing to excessive ultrasonic delamination, it is necessary to adopt SBSD strategy. Briefly, the delaminated f-$Ti_3C_2T_x$ nanosheets supernatant is collected in time to avoid generation of fragments under excessive sonication (Fig. S3 in the ESM), and the traditional sediments are proceeded with ultrasonic delamination after adding dispersant water. Repeating ultrasonic treatment and supernatant collection until the color of the supernatant is nearly clear, implying there is no further exfoliated f-$Ti_3C_2T_x$ from residuals. SBSD strategy can greatly increase the yield of the f-$Ti_3C_2T_x$ (72%) nanosheets, and final sediments can be reduced to 28% from traditional 85% in weight percent.

The fresh $Ti_3C_2T_x$ MXenes supernatant colloids are stable due to electrostatic repulsion between negatively charged MXenes nanosheets, endowed by the presence of the surface functional groups (–OH, –F, and –O) [42–44]. SPF phenomenon occurs once the electrostatic equilibrium is broken with addition of cations (Fig. S4 in the ESM) [45]. Considering the subsequent simple volatilization removability, diluted hydrochloric acid and ammonium salt solution can be selected as flocculants in this work. Upon addition of flocculant, cations were attracted to the surface of f-$Ti_3C_2T_x$, leading to destruction of electrostatic repulsion equilibrium state, and eventually complete electrostatic flocculation. After removing most of the water via flocculation process, the fast preparation of MXenes powders and MXenes films can be achieved via freeze-drying and vacuum-assisted filtration, respectively. The processes of flocculation can be further accelerated through MSPF with assistance of appropriate low speed centrifugation. In addition, for the hierarchical utilization of the raw MXenes, a mass of final sediments (28%) collected after MXenes delamination is selected as starting material to prepare MXenes-derived nanofibers through subsequent AHT. The composition of the nanofibers can be varied from potassium titanate ($K_2Ti_8O_{17}$, KTO) to sodium titanate (NTO) [46], depending on the condition of the process. By controlling the reaction time, 1D nanowires/2D nanosheet heterostructure with controllable nanofiber content can be obtained. If further prolong reaction time, final MXenes sediments can be completely converted into MXenes-derived nanofibers.

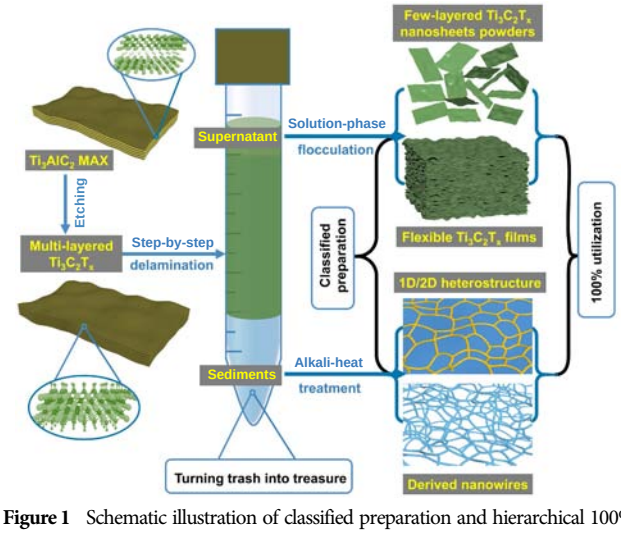

Figure 1 Schematic illustration of classified preparation and hierarchical 100% utilization of multi-layered MXenes, taking $Ti_3C_2T_x$ MXene as an example. In short, after delamination, the collected $Ti_3C_2T_x$ supernatant can be fast prepared into few-layered or even single-layered $Ti_3C_2T_x$ powders, flexible films. $Ti_3C_2T_x$ sediments can be alkalized into nanowires, leading to 100% utilization of raw multi-layered MXenes.

XRD results (Fig. 2(a)) show that Al layers are completely removed after HF etching which can be demonstrated by the disappearance of peak at 39° and the overall left shift of the remaining peaks (Fig. 2(b)), indicating the successful preparation of m-$Ti_3C_2T_x$ MXenes [39]. After treated in TMAOH, the XRD patterns of prepared f-$Ti_3C_2T_x$ powders, films, and final sediments are basically the same, indicating the "pillaring" and ultrasonic delamination process will not destroy the phase structure (Figs. 2(a) and 2(b)). After TMAOH intercalation, the (002) peak position shows obvious movement toward left compared with m-$Ti_3C_2T_x$, indicating larger TMA^+ ion groups are intercalated between the layers, leading to an enlargement of interlayer spacing. After alkalization treatment, interlayered TMA^+ is replaced by small K^+ or Na^+ via ion exchange, which is consistent with the right shift of (002) peak, indicating contraction of the interlayer spacing (Fig. 2(b)). Although the alkalized sample from final sediments exhibits basically the same XRD pattern as above-mentioned samples, some chemical changes occur during the AHT process. The (002) peak of $Ti_3C_2T_x$ is so strong that some useful signals are obscured. For this reason, the XRD results were re-displayed in different ranges. As shown in Fig. 2(c), new diffraction peaks can be observed after AHT process of 2 days. Moreover, the diffraction peaks of $Ti_3C_2T_x$ still exist in the sample. Hence, a possible reaction mechanism during AHT process is that: AHT will activate a gentle chemical reaction of $Ti_3C_2T_x$, leading to formation of heterostructure composed of $Ti_3C_2T_x$ and new components. The reaction during AHT process deserves further exploration and will be in-depth discussed in the following sections.

Compared with compact Ti_3AlC_2 MAX phases (Fig. S5 in the ESM), m-$Ti_3C_2T_x$ shows a typical loose accordion-like morphology (Fig. 3(a) and Figs. S6(a)–S6(c) in the ESM), consistent with previous reports [47]. Impressively, the f-$Ti_3C_2T_x$ nanosheets without any re-stacking issues can be obtained via SPF method and subsequent annealing process to remove the introduced ammonium ion or hydrogen ion, as well as terminated –OH groups (Eqs. (1) and (2)). The f-MXenes and s-MXenes nanosheet powders can be characterized from the minimum magnification of 400 times under SEM (Figs. 3(b)–3(f) and Figs. S6(d)–S6(f) in the ESM), and obvious few-layered nanosheets can be observed without re-stacking phenomenon in all randomly selected area. It is well known that delaminated MXenes supernatant can be inevitably oxidized in oxygen atmosphere and dispersant water [18]. SPF method enables convenient and rapid

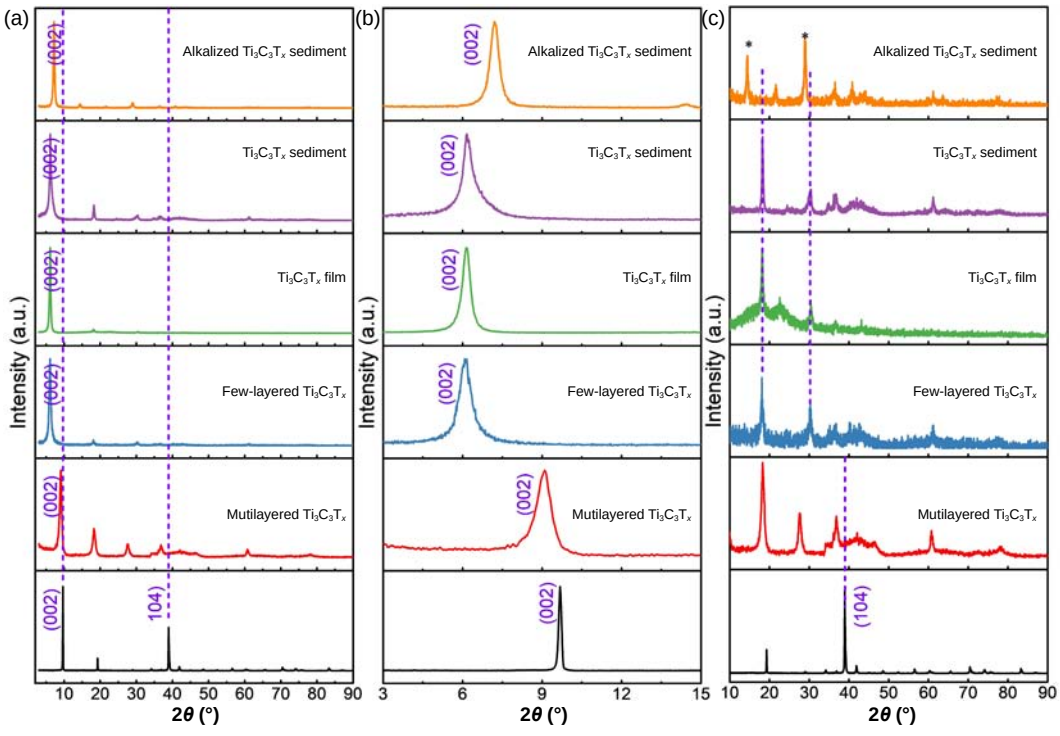

Figure 2 XRD patterns of related samples at different diffraction angle ranges, including Ti_3AlC_2, multi-layered $Ti_3C_2T_x$, few-layered $Ti_3C_2T_x$ powders, $Ti_3C_2T_x$ films, $Ti_3C_2T_x$ sediments, and alkalized $Ti_3C_2T_x$ sediments (alkalization for 2 days in aqueous solution). (a) 2θ from 3° to 90°, (b) 2θ from 3° to 15°, and (c) 2θ from 10° to 90°.

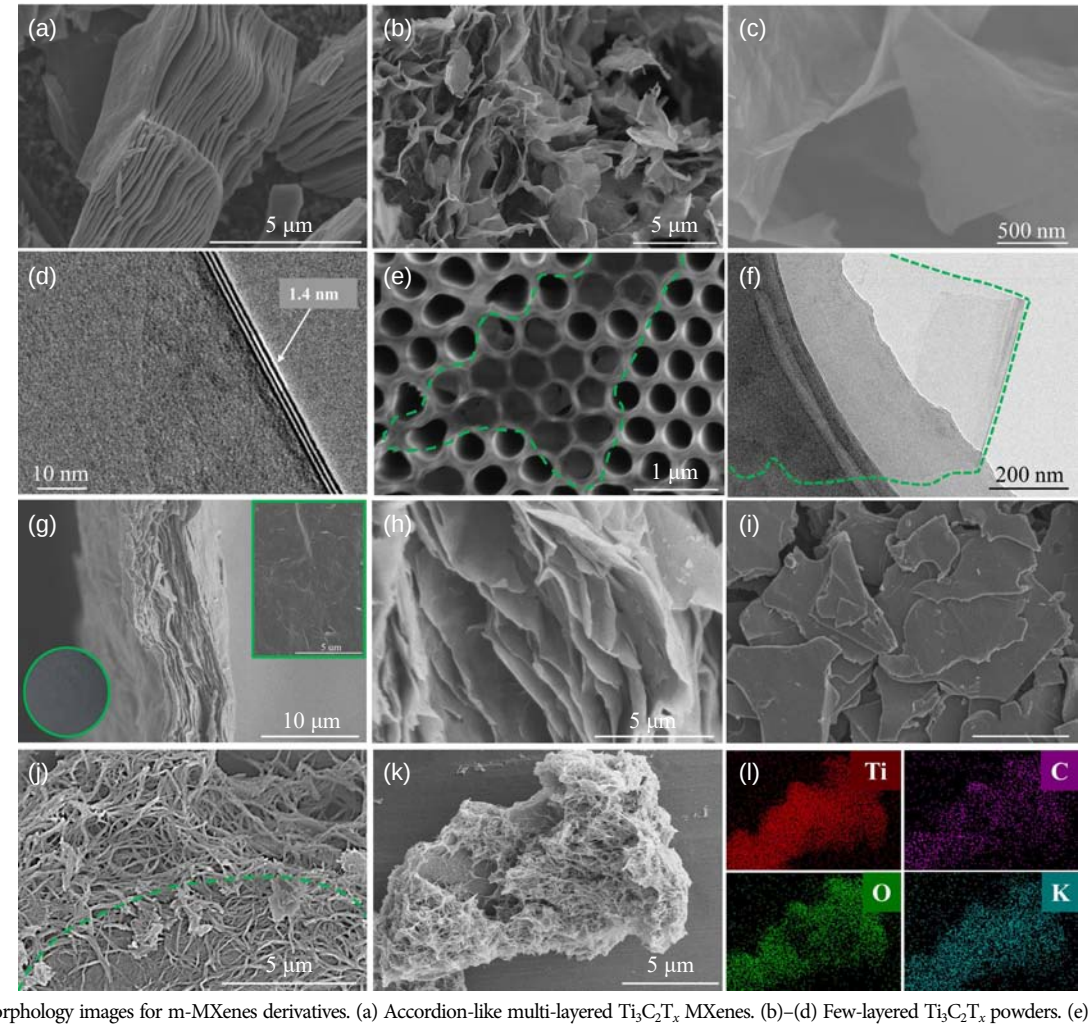

Figure 3 Morphology images for m-MXenes derivatives. (a) Accordion-like multi-layered $Ti_3C_2T_x$ MXenes. (b)–(d) Few-layered $Ti_3C_2T_x$ powders. (e) Single-layered $Ti_3C_2T_x$ on AAO films. (f) TEM image of single-layered $Ti_3C_2T_x$. (g)–(h) Cross-section images of $Ti_3C_2T_x$ films based on SPF method, and the inset in the lower left corner of (g) is photograph picture of $Ti_3C_2T_x$ films and higher right corner of (g) is top-view image of $Ti_3C_2T_x$ films. (i) Tile-like $Ti_3C_2T_x$ MXenes sediments after delamination. (j) Heterostructure derived from $Ti_3C_2T_x$ sediments after alkali-heat treatment for 6 days. (k)–(l) Overall morphology of the heterostructure and corresponding SEM-EDS element mappings.

preparation of f-MXenes and s-MXenes powders, which can be stored in water and oxygen free environment. Consequently, the SPF method is of great significance for the development of MXenes, which not only fundamentally solves the re-stacking problem of delaminated MXenes, but also avoids their oxidation during storage.

$$[NH_4^+]\,[OH^-] \rightleftharpoons NH_3 + H_2O \quad (1)$$

$$[H^+]\,[OH^-] \rightleftharpoons H_2O \quad (2)$$

There are already a lot of previous reports about flexible self-supporting MXenes-based films, prepared via vacuum-assisted filtration process [34–36]. However, due to serious re-stacking of delaminated f-MXenes nanosheets, the filtration process is very time-consuming. The restacked MXenes nanosheets severely restrict the passage of water flow, resulting in very low production efficiency for a dedicated vacuum pump. Since the SPF method can effectively solve the re-stacking problem of f-MXenes and generate unimpeded channel for water flow, the flocculation mixture can be fast filtrated to prepare free-standing MXenes films. Porous structure can be clearly observed from the cross-sectional view of the films (Figs. 3(g) and 3(h)), showing porous multi-channel structure compared with densely stacked and aggregated MXenes nanosheets prepared by the conventional method [10, 48, 49]. After solution-phase flocculation, MXenes films can be produced within 5 min by filtration, which is only 1/60 to 1/120 of the time compared with the conventional method (5–10 h). The production efficiency can be further significantly improved in the preparation of multiple films, strongly demonstrating the effectiveness of the SPF method in preparing free-standing MXenes films.

The final sediments, collected after centrifugation, show obvious tile-like morphology (Fig. 3(i) and Figs. S6(g)–S6(i) in the ESM). These sediments are essentially un-exfoliated $Ti_3C_2T_x$ MXenes based on the XRD results (Fig. 2(a)). After alkali-heat treatment for 6 d in KOH aqueous solution, it generates interconnected nanowires framework closely adhered to the tile-like substrate. The heterostructure can be clearly observed through SEM image as shown in Fig. 3(j), in which the nanowire framework and the bulk substrate can be roughly divided by the tagged line. The elemental mapping characterization reveals the even distribution of Ti, C, O, and K elements in the sample, implying the composition change after AHT process (Figs. 3(k) and 3(l) and Fig. S7 in the ESM). Furthermore, the SEM-energy dispersive spectrometer (SEM-EDS) shows there are 35.45 wt.% Ti and 13.21 wt.% C in the sample (Table S1 in the ESM), corresponding to a Ti:C molar ratio about 0.67. The discrepancy compared to the stoichiometric ratio of Ti_3C_2 indicates it probably forms new chemicals after alkali-heat treatment. Therefore, the AHT product consists of two parts, including 2D m-MXenes subgrade and 1D nanowire attachment, which indicates the alkalized sediments are heterostructure and chemical reactions occur during AHT. As far as we know, the AHT-induced preparation of nanowires based on the sediments has not been reported. Therefore, it is necessary to design experiment to systematically analyze the composition of MXenes-derived nanowires.

As we know, the chemical reaction product is determined by the chemical components of reactant and reaction condition, regardless of morphology (Fig. 4), which can only affect reaction kinetic. Hence, in order to assure the complete transformation of the reactant, the $Ti_3C_2T_x$ sediments were replaced by f-$Ti_3C_2T_x$ to obtain final alkalized samples. After the same alkali-heat treatment for 3 d, it was found that the colors of the f-$Ti_3C_2T_x$ and sediment suspensions are quite different (ochre for f-$Ti_3C_2T_x$ and red-brown for sediments), as well as the XRD result of these two samples (Fig. S8 in the ESM and Figs. 5(a) and 5(b)). The XRD pattern of the product derived from f-$Ti_3C_2T_x$ after AHT for 3 d well matches with the PDF card of $K_2Ti_8O_{17}$ (KTO) (PDF: #84-2057), and no (002) peak corresponding to $Ti_3C_2T_x$ is observed, indicating the full reaction of the reactant. Impressively, when the alkalization-heat reaction time is extended to 10 days, ochre solution can also be observed for $Ti_3C_2T_x$ sediments, of which the XRD pattern also coincides well with the standard peak of $K_2Ti_8O_{17}$ (Fig. 5(a)). Therefore, it can be affirmed that the final nanowires synthesized under such AHT condition are potassium titanate ($K_2Ti_8O_{17}$), and f-$Ti_3C_2T_x$ shows better chemical reaction kinetics compared with $Ti_3C_2T_x$ sediments. Besides, final $Ti_3C_2T_x$ sediments can also be alkalized to form sodium titanate when NaOH was used in AHT process (Fig. S9 in the ESM).

In order to explore the reaction mechanism, a series of contrast experiments were carried out based on different AHT time. We denote alkalized sediments as KTO-0, KTO-2, KTO-4, KTO-6, KTO-8, KTO-10 to describe fresh $Ti_3C_2T_x$ sediments and alkalized sediments in KOH solution for 2, 4, 6, 8, and 10 days, respectively. According to the *ex-situ* SEM images, with the AHT time increasing, nanowires grow continuously until no residues of MXenes substrate, indicating a surface reaction process (Figs. 4(a)–4(f)). The evolution process of the morphology can be vividly depicted by the schematic in Fig. 4(g). More detailed morphology and structure information of the AHT product was collected through TEM test. As shown in Fig. 4(h), due to influence of water molecules, external MXenes can be gradually oxidized and degraded as titanium dioxide, leading to an intermediate layer composed of nanoparticles, which can further self-assemble into short nanowires of potassium titanate. With the extension of AHT process, all of nanoparticles were self-assembled, converted into longer 3D intertwined nanowires of $K_2Ti_8O_{17}$, demonstrating the evolution from bulk to nanoparticle and further to nanofiber during AHT process. The formation of nanoparticles accounts for the surface roughness in initial AHT product as shown in Fig. 4(b). After AHT for 10 days, the bulk completely converts to interwoven KTO nanofibers (Fig. 4(i) and Fig. S10 in the ESM). As shown in Figs. 4(i) and 4(j), the polycrystalline KTO nanofiber exhibits lamellar structure with a high interlamellar spacing of 0.84 nm, and lattice spacing of 0.22 nm corresponds to (404) crystal plane of $K_2Ti_8O_{17}$, consistent with the XRD result.

As shown in Fig. 5(b) and Fig. S11 in the ESM, *ex-situ* XRD results can directly reflect the evolution of chemical compositions during the process. In the early stage of alkalization, the $Ti_3C_2T_x$ sediments transform to titanium oxide intermedium under alkali thermal oxidation. Afterwards, the diffraction peaks corresponding to the intermedium decay continuously, implying further transformation from intermedium to final product (Fig. S11(c) in the ESM). Owing to relatively low content and crystallinity, the diffraction signal of KTO can be observed until reaction time reaches up to 6 d (KTO-6). As reaction time goes on, the characteristic (002) peak of MXenes attenuates continuously, while the characteristic peaks of KTO constantly intensify, which is highly consistent with *ex-situ* SEM images (Figs. 4(a)–4(f)). In addition, the BET specific surface areas (SSA) of the products increase as the alkalization reaction progresses (Fig. 5(c) and Fig. S12 in the ESM), corresponding to the increase of nanowires content, which can be reflected in *ex-situ* SEM images (Figs. 4(a)–4(f)). The high SSA promises excellent properties of the final KTO nanowires in various applications [50]. Figure 5(d) and Fig. S13 in the ESM show the Raman spectrum of fresh $Ti_3C_2T_x$ sediment, alkalized KTO-6, and KTO-10. In the

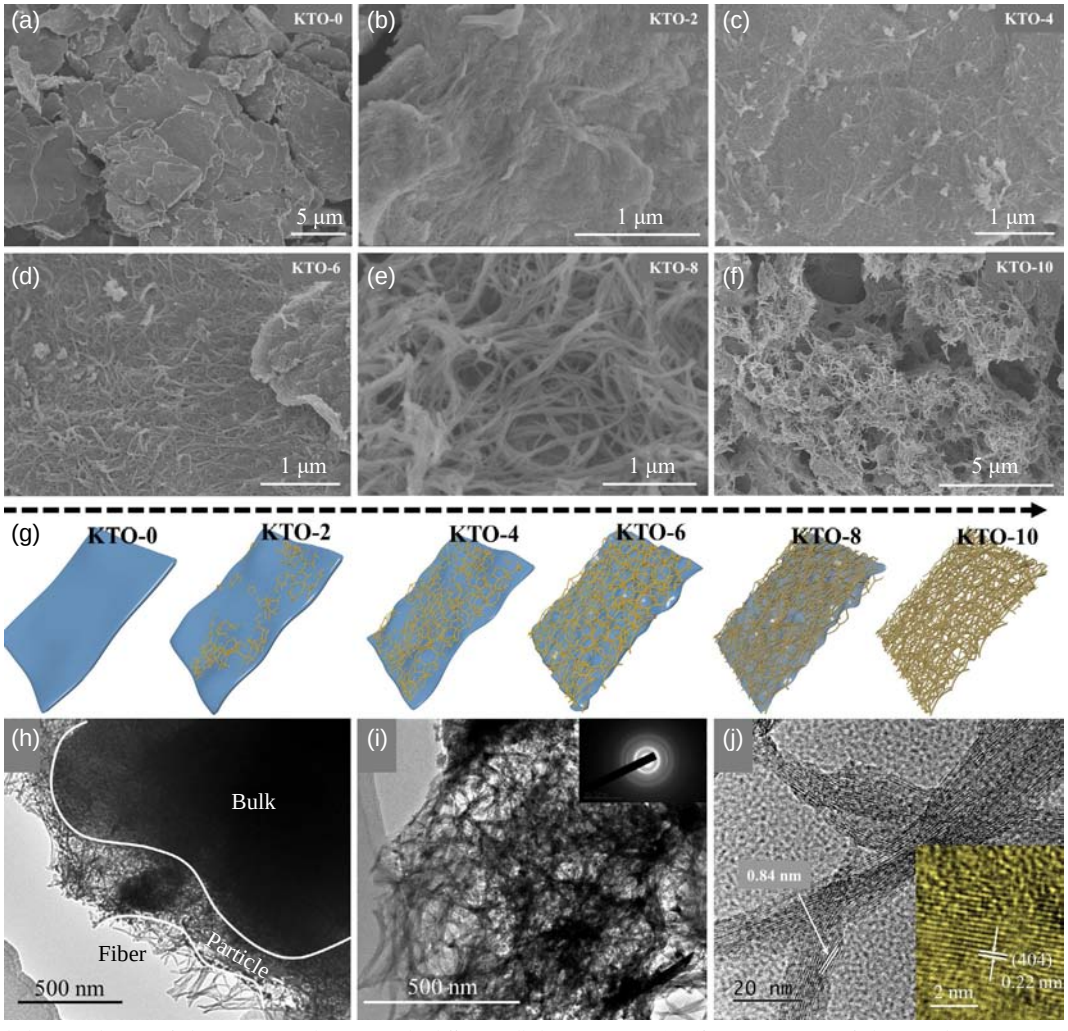

Figure 4 Morphology evolution of the $Ti_3C_2T_x$ sediments with different alkalization time. (a)–(f) SEM images of the samples. (g) Schematic illustration transformation of $Ti_3C_2T_x$ sediments during alkalization process. (h) TEM image of KTO-6. (i) TEM image of KTO-10 and inset is SAED patterns. (j) High resolution TEM (HR-TEM) image of KTO-10.

range of low shift, four peaks of $Ti_3C_2T_x$ sediment located at 150, 260, 401, and 598 cm^{-1} correspond to vibration modes of non-stoichiometric Ti–C after etching and exfoliation process [51, 52]. Obviously different from fresh $Ti_3C_2T_x$ sediment, there are several newly characteristic peaks assigned to Ti–O–K vibrations (438 and 650 cm^{-1}), Ti–O–Ti stretching vibration (280 cm^{-1}), and Ti–O stretching vibration (196, 836, and 915 cm^{-1}) in the results of KTO-6 [53], nearly the same as that of KTO-10, except that Ti–C can be maintained at 142 cm^{-1} of KTO-6 while completely disappeared at KTO-10, indicating thorough transformation from $Ti_3C_2T_x$ to KTO. C signals of two peaks (D peak at ~ 1,356 cm^{-1} and G peak at ~ 1,570 cm^{-1}) were also evolved with AHT process, the I_D/I_G diminished gradually. There is no signal of CO_3^{2-} in the final solution of KTO (Fig. S14 in the ESM), suggesting that C in $Ti_3C_2T_x$ may be evaporated as carbon dioxide during AHT process [54].

To investigate chemical bonding of MXenes during transformation reaction, XPS measurements were performed (Figs. 5(e)–5(h)). As clearly exhibited in the full spectra and K 2p spectra of the fresh MXenes sediments KTO-0, KTO-6, and KTO-10, the K signals appear and F peak almost disappears after alkalization process, indicating the chemical changes during AHT process. The follow-up study of high-resolution spectra can convincingly demonstrate the formation of new chemicals. There are only Ti–C and C–C bonds detected in the C 1s spectrum of fresh $Ti_3C_2T_x$ sediments (Fig. 5(g)), nevertheless, the Ti–C bond significantly weakens, while C–O and C=O chemical bonds arise after AHT for 6 days, indicating the oxidative damage of MXenes structure. The Ti–C chemical bond disappears after AHT for 10 d, indicating the thorough transformation of $Ti_3C_2T_x$ sediments to KTO nanowires. The transformation from $Ti_3C_2T_x$ sediments to 1D/2D heterostructure and final KTO nanowires can also be concluded from the evolution of Ti 2p spectra, where Ti–C peak fades gradually until disappears while Ti–O peak enhances with the reaction time increasing (Fig. 5(f)). In addition, the evolution of O 1s peak further confirms the oxidation of the $Ti_3C_2T_x$ sediments (Fig. S15 in the ESM). Therefore, the final product can be attributed to compounds of K, Ti, and O, which is consistent with the XRD results. As previously reported, the Ti–C bonds of $Ti_3C_2T_x$ in hot aqueous alkali will be destroyed by interaction of water molecules and terminated functional groups [54, 55], and the formed titanium oxide particles on surface can further react with alkali solution to form alkali titanate nanowires [56, 57]. Hence, it is speculated that the entire reaction process includes two steps: First, $Ti_3C_2T_x$ is gradually oxidized to titanium dioxide nanoparticles, and then titanium dioxide is converted into final KTO nanowires.

The f-$Ti_3C_2T_x$ powders and flexible self-supporting f-$Ti_3C_2T_x$ films have been widely used in various fields with outstanding performance [58], together with extensive reviews up to date (Fig. S1 in the ESM) [34–36], demonstrating their application potential [24, 59]. In contrast, there are only a handful studies about MXenes-derived nanofibers. Nevertheless, the vast application of these nanofibers has emerged [60–62]. In composition, the

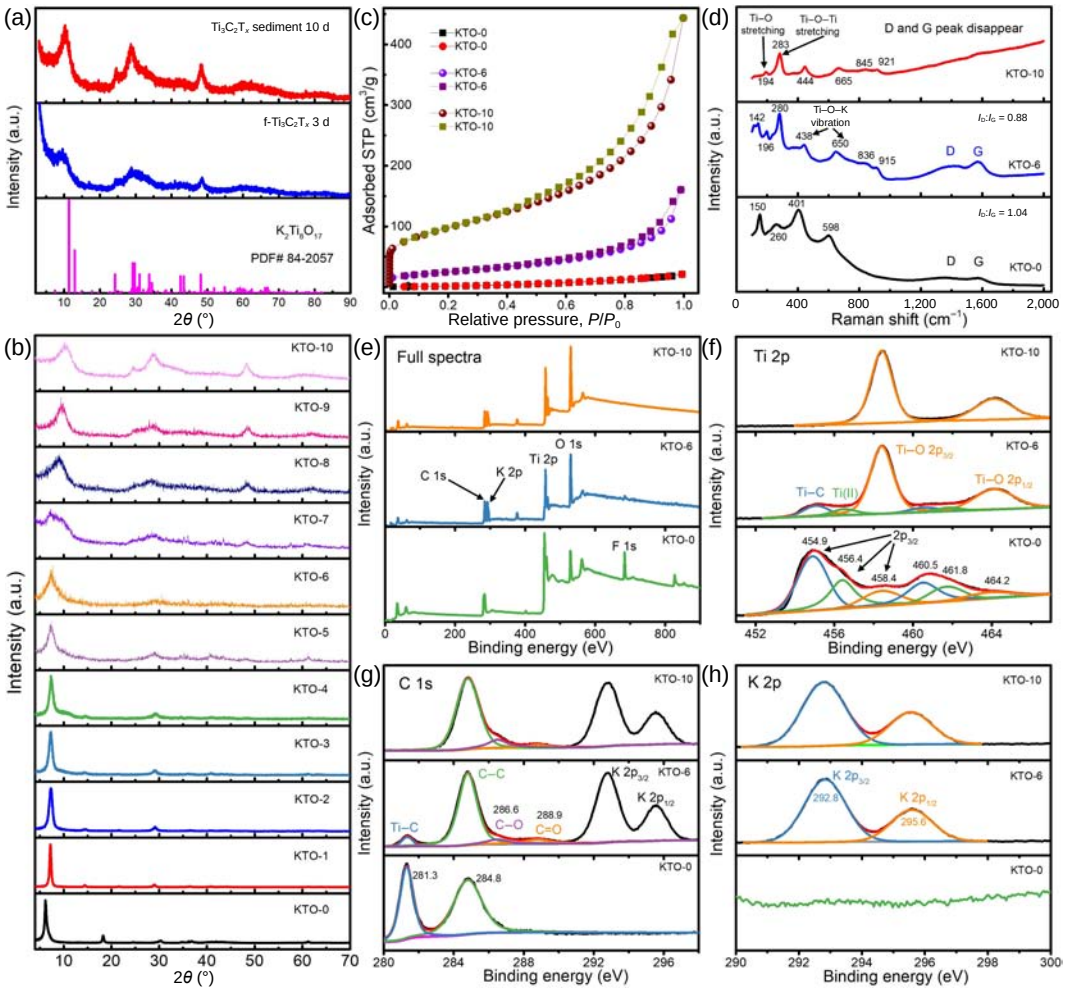

Figure 5 (a) XRD patterns of alkalized samples. (b) *Ex-situ* XRD patterns of alkalized $Ti_3C_2T_x$ sediments with different alkalization time. (c) N_2 adsorption–desorption isotherm curve. (d) Raman spectra. (e) XPS study of full spectra. (f) Ti 2p, (g) C 1s, and (h) K 2p spectra of the related derivates.

MXenes-derived nanowire can be alkali metal titanate and MXenes themselves, depending on the condition of the alkalization process (oxidation for alkali metal titanate and inert environment for MXenes themselves) [56, 63–65]. It should be noted that MXenes can be oxidized and degraded as TiO_2 in the presence of dissolved oxygen or H_2O [18]. As a result, most of the derived nanofibers are different alkali metal titanates nanowires, except for inert environment protection [63]. Alkali metal titanates are also closely related to detailed alkali solutions of NaOH or KOH, (NaOH for NTO and KOH for KTO) [46, 65]. The various MXenes-derived nanowires that have been currently reported are summarized in Table S2 in the ESM. For example, sodium titanate of $Na_3Ti_5O_{12}$-MXene hybrid can be obtained after NaOH oxidation process with appropriate time, effectively preventing Na dendrites and resulting in stable cycling performance [56]. Sandwich-like $Na_{0.23}TiO_2$ nanobelt/Ti_3C_2 MXenes composites can be directly used as anodes for lithium/sodium-ion batteries, displaying superior cycling stability and rate performance [53]. Complete $Ti_3C_2T_x$-derived potassium titanate of $K_2Ti_8O_{17}$ nanowires can be obtained after KOH alkalization, delivering a higher capacity of 145 mAh·g^{-1} in potassium ion micro-supercapacitors [65].

Importantly, alkalization of MXenes results in the formation of unique 3D architecture heterostructure composed of 1D nanowires and 2D nanosheets. The heterostructure shows salient advantages when applied in energy storage fields [66–68], including the fact that 1D nanowires enable short ion diffusion path and accommodate volumetric strain while 2D MXenes nanosheets endow high conductivity and fast interfacial electron transfer. Moreover, 3D interconnected architecture with adequate space can promote electrolyte penetration, ion transport, and avoid aggregation of active materials. As result, $Ti_3C_2T_x$-derived nanowires of sodium/potassium titanate are attractive for Na/K storage owing to their unique preparation–structure–function relationships [56, 65]. In this work, we found that usually discarded $Ti_3C_2T_x$ sediments can be alkalized as nanowires, achieving 100% hierarchical utilization of accordion-like m-$Ti_3C_2T_x$ (as shown in Fig. 1 and Fig. S2 in the ESM). We believe this work can accelerate the industrialization application of MXenes [69, 70].

4 Conclusions

In summary, focusing on basic preparation of various $Ti_3C_2T_x$ MXenes derivatives and utilization of discarded $Ti_3C_2T_x$ sediments, we realize the classified, rapid, and large-scale preparation of various $Ti_3C_2T_x$ derivatives with 100% utilization of raw MXenes. Remarkably, the yield of the f-$Ti_3C_2T_x$ nanosheets can be improved up to 72% by stepwise delamination towards traditional $Ti_3C_2T_x$ sediments, without formation of fragment which is common in traditional excessive ultrasonic exfoliation. Furthermore, solution-phase flocculation was applied via addition of diluted hydrochloric acid or ammonium salts to thoroughly solve the re-stacking phenomenon of f-$Ti_3C_2T_x$ MXenes, leading to fast preparation of f-$Ti_3C_2T_x$ powders and self-supporting films. More importantly, the final $Ti_3C_2T_x$ sediments, which are directly discarded in previous works, can be re-utilized by transforming into $Ti_3C_2T_x$-derived nanowires through AHT. It is found that the

AHT-induced surface evolution will generate MXenes-derived 1D/2D nanowire/nanosheet heterostructure, and finally form pure nanowires after sufficient AHT time. 100% utilization of raw m-MXenes can be achieved based on the proposed guidelines of classified preparation and hierarchical exploitation toward raw m-MXenes. It is exciting that the key points, including stepwise delamination, solution-phase flocculation, and alkali-heat treatment toward final MXenes sediments, can realize the hierarchical 100% utilization of MXenes, together with fundamental solutions toward re-stacking, oxidation during storage, and low yields of f-MXenes. We believe this work can bring new applications and promote the practical commercial process of various MXenes.

Acknowledgments

The authors are grateful for the financial support by the National Natural ScienceFoundation of China (No. 51901206) and the fund from Taihu Electric Corporation 0001.

Electronic Supplementary Material: Supplementary material (SEM images of multi-layered, few-layered $Ti_3C_2T_x$ MXene, TEM images of alkalized potassium titanate derived from $Ti_3C_2T_x$ sediments, the pore size distribution and N_2 adsorption–desorption isotherm curve of $Ti_3C_2T_x$ sediments derived nanowires, and XRD patterns of the related samples) is available in the online version of this article at https://doi.org/10.1007/s12274-021-3847-4.

References

[1] Anasori, B.; Lukatskaya, M. R.; Gogotsi, Y. 2D metal carbides and nitrides (MXenes) for energy storage. *Nat. Rev. Mater.* **2017**, *2*, 16098.

[2] Naguib, M.; Kurtoglu, M.; Presser, V.; Lu, J.; Niu, J. J.; Heon, M.; Hultman, L.; Gogotsi, Y.; Barsoum, M. W. Two-dimensional nanocrystals produced by exfoliation of Ti_3AlC_2. *Adv. Mater.* **2011**, *23*, 4248–4253.

[3] Sokol, M.; Natu, V.; Kota, S.; Barsoum, M. W. On the chemical diversity of the MAX phases. *Trends Chem.* **2019**, *1*, 210–223.

[4] Nan, J. X.; Guo, X.; Xiao, J.; Li, X.; Chen, W. H.; Wu, W. J.; Liu, H.; Wang, Y.; Wu, M. H.; Wang, G. X. Nanoengineering of 2D MXene-based materials for energy storage applications. *Small* **2021**, *17*, 1902085.

[5] Zhao, D. Y.; Zhao, R. Z.; Dong, S. H.; Miao, X. G.; Zhang, Z. W.; Wang, C. X.; Yin, L. W. Alkali-induced 3D crinkled porous Ti_3C_2 MXene architectures coupled with NiCoP bimetallic phosphide nanoparticles as anodes for high-performance sodium-ion batteries. *Energy Environ. Sci.* **2019**, *12*, 2422–2432.

[6] Sun, Y.; Zhou, Y. J.; Liu, Y.; Wu, Q. Y.; Zhu, M. M.; Huang, H.; Liu, Y.; Shao, M. W.; Kang, Z. H. A photoactive process cascaded electrocatalysis for enhanced methanol oxidation over Pt-MXene-TiO_2 composite. *Nano Res.* **2020**, *13*, 2683–2690.

[7] Hui, X. B.; Ge, X. L.; Zhao, R. Z.; Li, Z. Q.; Yin, L. W. Interface chemistry on MXene-based materials for enhanced energy storage and conversion performance. *Adv. Funct. Mater.* **2020**, *30*, 2005190.

[8] Wei, C. L.; Wang, Y. S.; Zhang, Y. C.; Tan, L. W.; Qian, Y.; Tao, Y.; Xiong, S. L.; Feng, J. K. Flexible and stable 3D lithium metal anodes based on self-standing MXene/COF frameworks for high-performance lithium-sulfur batteries. *Nano Res.* **2021**.

[9] Zhao, R. Z.; Di, H. X.; Wang, C. X.; Hui, X. B.; Zhao, D. Y.; Wang, R. T.; Zhang, L. Y.; Yin, L. W. Encapsulating ultrafine Sb nanoparticles in Na^+ pre-intercalated 3D porous $Ti_3C_2T_x$ MXene nanostructures for enhanced potassium storage performance. *ACS Nano* **2020**, *14*, 13938–13951.

[10] Fang, Y. Z.; Zhang, Y.; Zhu, K.; Lian, R. Q.; Gao, Y.; Yin, J. L.; Ye, K.; Cheng, K.; Yan, J.; Wang, G. L. et al. Lithiophilic three-dimensional porous $Ti_3C_2T_x$-rGO membrane as a stable scaffold for safe alkali metal (Li or Na) anodes. *ACS Nano* **2019**, *13*, 14319–14328.

[11] Wang, H.; Cao, J. J.; Zhou, Y. J.; Wang, X.; Huang, H.; Liu, Y.; Shao, M. W.; Kang, Z. H. Carbon dots modified $Ti_3C_2T_x$-based fibrous supercapacitor with photo-enhanced capacitance. *Nano Res.* **2021**.

[12] Guo, D. Z.; Li, X.; Jiao, Y. Q.; Yan, H. J.; Wu, A. P.; Yang, G. C.; Wang, Y.; Tian, C. G.; Fu, H. G. A dual-active Co-CoO heterojunction coupled with Ti_3C_2-MXene for highly-performance overall water splitting. *Nano Res.* **2021**.

[13] Wang, Z. H.; Yang, L. X.; Zhou, Y.; Xu, C.; Yan, M.; Wu, C. NiFe LDH/MXene derivatives interconnected with carbon fabric for flexible electromagnetic wave absorption. *ACS Appl. Mater. Interfaces* **2021**, *13*, 16713–16721.

[14] Cao, W. T.; Ma, C.; Tan, S.; Ma, M. G.; Wan, P. B.; Chen, F. Ultrathin and flexible CNTs/MXene/Cellulose nanofibrils composite paper for electromagnetic interference shielding. *Nano-Micro Lett.* **2019**, *11*, 72.

[15] Hu, D. W.; Wang, S. Q.; Zhang, C.; Yi, P. S.; Jiang, P. K.; Huang, X. Y. Ultrathin MXene-aramid nanofiber electromagnetic interference shielding films with tactile sensing ability withstanding harsh temperatures. *Nano Res.* **2021**.

[16] Guo, X.; Zhang, W. X.; Zhang, J. Q.; Zhou, D.; Tang, X.; Xu, X. F.; Li, B. H.; Liu, H.; Wang, G. X. Boosting sodium storage in two-dimensional phosphorene/$Ti_3C_2T_x$ MXene nanoarchitectures with stable fluorinated interphase. *ACS Nano* **2020**, *14*, 3651–3659.

[17] Cao, Y. P.; Chen, H.; Shen, Y. P.; Chen, M.; Zhang, Y. L.; Zhang, L. Y.; Wang, Q.; Guo, S. J.; Yang, H. SnS_2 nanosheets anchored on nitrogen and sulfur co-doped MXene sheets for high-performance potassium-ion batteries. *ACS Appl. Mater. Interfaces* **2021**, *13*, 17668–17676.

[18] Zhang, S. L.; Han, W. Q. Recent advances in MXenes and their composites in lithium/sodium batteries from the viewpoints of components and interlayer engineering. *Phys. Chem. Chem. Phys.* **2020**, *22*, 16482–16526.

[19] Jiang, X. T.; Kuklin, A. V.; Baev, A.; Ge, Y. Q.; Ågren, H.; Zhang, H.; Prasad, P. N. Two-dimensional MXenes: From morphological to optical, electric, and magnetic properties and applications. *Phys. Rep.* **2020**, *848*, 1–58.

[20] Alhabeb, M.; Maleski, K.; Anasori, B.; Lelyukh, P.; Clark, L.; Sin, S.; Gogotsi, Y. Guidelines for synthesis and processing of two-dimensional titanium carbide ($Ti_3C_2T_x$ MXene). *Chem. Mater.* **2017**, *29*, 7633–7644.

[21] Naguib, M.; Mochalin, V. N.; Barsoum, M. W.; Gogotsi, Y. 25th anniversary article: MXenes: A new family of two-dimensional materials. *Adv. Mater.* **2014**, *26*, 992–1005.

[22] Li, Y. B.; Shao, H.; Lin, Z. F.; Lu, J.; Liu, L. Y.; Duployer, B.; Persson, P. O. Å.; Eklund, P.; Hultman, L.; Li, M. et al. A general lewis acidic etching route for preparing MXenes with enhanced electrochemical performance in non-aqueous electrolyte. *Nat. Mater.* **2020**, *19*, 894–899.

[23] Zhang, Q. X.; Lai, H. R.; Fan, R. Z.; Ji, P. Y.; Fu, X. L.; Li, H. High concentration of $Ti_3C_2T_x$ MXene in organic solvent. *ACS Nano* **2021**, *15*, 5249–5262.

[24] Jun, B. M.; Kim, S.; Heo, J.; Park, C. M.; Her, N.; Jang, M.; Huang, Y.; Han, J.; Yoon, Y. Review of MXenes as new nanomaterials for energy storage/delivery and selected environmental applications. *Nano Res.* **2019**, *12*, 471–487.

[25] Li, K.; Liang, M. Y.; Wang, H.; Wang, X. H.; Huang, Y. S.; Coelho, J.; Pinilla, S.; Zhang, Y. L.; Qi, F. W.; Nicolosi, V. et al. 3D MXene architectures for efficient energy storage and conversion. *Adv. Funct. Mater.* **2020**, *30*, 2000842.

[26] Li, M.; Lu, J.; Luo, K.; Li, Y. B.; Chang, K. K.; Chen, K.; Zhou, J.; Rosen, J.; Hultman, L.; Eklund, P. et al. Element replacement approach by reaction with lewis acidic molten salts to synthesize nanolaminated MAX phases and MXenes. *J. Am. Chem. Soc.* **2019**, *141*, 4730–4737.

[27] Yao, L.; Gu, Q. F.; Yu, X. B. Three-dimensional MOFs@MXene aerogel composite derived MXene threaded hollow carbon confined CoS nanoparticles toward advanced alkali-ion batteries. *ACS Nano* **2021**, *15*, 3228–3240.

[28] Zhu, J. T.; Wang, H.; Ma, L.; Zou, G. F. Observation of ambipolar

photoresponse from 2D MoS_2/MXene heterostructure. *Nano Res.* **2021**.

[29] Abdolhosseinzadeh, S.; Schneider, R.; Verma, A.; Heier, J.; Nüesch, F.; Zhang, C. F. Turning trash into treasure: Additive free MXene sediment inks for screen-printed micro-supercapacitors. *Adv. Mater.* **2020**, *32*, 2000716.

[30] Rajavel, K.; Yu, X. C.; Zhu, P. L.; Hu, Y. G.; Sun, R.; Wong, C. Exfoliation and defect control of two-dimensional few-layer MXene $Ti_3C_2T_x$ for electromagnetic interference shielding coatings. *ACS Appl. Mater. Interfaces* **2020**, *12*, 49737–49747.

[31] Tang, R. D.; Xiong, S.; Gong, D. X.; Deng, Y. C.; Wang, Y. C.; Su, L.; Ding, C. X.; Yang, L. H.; Liao, C. J. Ti_3C_2 2D MXene: Recent progress and perspectives in photocatalysis. *ACS Appl. Mater. Interfaces* **2020**, *12*, 56663–56680.

[32] Xie, X. Q.; Zhao, M. Q.; Anasori, B.; Maleski, K.; Ren, C. E.; Li, J. W.; Byles, B. W.; Pomerantseva, E.; Wang, G. X.; Gogotsi, Y. Porous heterostructured MXene/carbon nanotube composite paper with high volumetric capacity for sodium-based energy storage devices. *Nano Energy* **2016**, *26*, 513–523.

[33] Zhao, X. F.; Vashisth, A.; Prehn, E.; Sun, W. M.; Shah, S. A.; Habib, T.; Chen, Y. X.; Tan, Z. Y.; Lutkenhaus, J. L.; Radovic, M. et al. Antioxidants unlock shelf-stable $Ti_3C_2T_x$ (MXene) nanosheet dispersions. *Matter* **2019**, *1*, 513–526.

[34] Li, J.; Li, X. ; Van der Bruggen, B. An MXene-based membrane for molecular separation. *Environ. Sci.: Nano* **2020**, *7*, 1289–1304.

[35] Gao, L. F.; Li, C.; Huang, W. C.; Mei, S.; Lin, H.; Ou, Q.; Zhang, Y.; Guo, J.; Zhang, F.; Xu, S. X. et al. MXene/polymer membranes: Synthesis, properties, and emerging applications. *Chem. Mater.* **2020**, *32*, 1703–1747.

[36] Karahan, H. E.; Goh, K.; Zhang, C. F.; Yang, E.; Yıldırım, C.; Chuah, C. Y.; Ahunbay, M. G.; Lee, J.; Tantekin-Ersolmaz, Ş. B.; Chen, Y. et al. MXene materials for designing advanced separation membranes. *Adv. Mater.* **2020**, *32*, 1906697.

[37] Fu, Z. H.; Wang, N.; Legut, D.; Si, C.; Zhang, Q. F.; Du, S. Y.; Germann, T. C.; Francisco, J. S.; Zhang, R. F. Rational design of flexible two-dimensional MXenes with multiple functionalities. *Chem. Rev.* **2019**, *119*, 11980–12031.

[38] Wei, C. L.; Tao, Y.; An, Y. L.; Tian, Y.; Zhang, Y. C.; Feng, J. K.; Qian, Y. T. Recent advances of emerging 2D MXene for stable and dendrite-free metal anodes. *Adv. Funct. Mater.* **2020**, *30*, 2004613.

[39] Zhang, S. L.; Ying, H. J.; Guo, R. N.; Yang, W. T.; Han, W. Q. Vapor deposition red phosphorus to prepare nitrogen-doped $Ti_3C_2T_x$ MXenes composites for lithium-ion batteries. *J. Phys. Chem. Lett.* **2019**, *10*, 6446–6454.

[40] Huang, P. F.; Zhang, S. L.; Ying, H. J.; Yang, W. T.; Wang, J. L.; Guo, R. N.; Han, W. Q. Fabrication of Fe nanocomplex pillared few-layered $Ti_3C_2T_x$ MXene with enhanced rate performance for lithium-ion batteries. *Nano Res.* **2021**, *14*, 1218–1227.

[41] Shekhirev, M.; Shuck, C. E.; Sarycheva, A.; Gogotsi, Y. Characterization of MXenes at every step, from their precursors to single flakes and assembled films. *Prog. Mater. Sci.* **2021**, *120*, 100757.

[42] Zhang, F.; Guo, X.; Xiong, P.; Zhang, J. Q.; Song, J. J.; Yan, K.; Gao, X. C.; Liu, H.; Wang, G. X. Interface engineering of MXene composite separator for high-performance Li-Se and Na-Se batteries. *Adv. Energy Mater.* **2020**, *10*, 2000446.

[43] Guo, X.; Zhang, J. Q.; Song, J. J.; Wu, W. J.; Liu, H.; Wang, G. X. MXene encapsulated titanium oxide nanospheres for ultra-stable and fast sodium storage. *Energy Storage Mater.* **2018**, *14*, 306–313.

[44] Tang, X.; Guo, X.; Wu, W. J.; Wang, G. X. 2D metal carbides and nitrides (MXenes) as high-performance electrode materials for lithium-based batteries. *Adv. Energy Mater.* **2018**, *8*, 1801897.

[45] Fan, Z. D.; Jin, J.; Li, C.; Cai, J. S.; Wei, C. H.; Shao, Y. L.; Zou, G. F.; Sun, J. Y. 3D-printed Zn-ion hybrid capacitor enabled by universal divalent cation-gelated additive-free Ti_3C_2 MXene ink. *ACS Nano* **2021**, *15*, 3098–3107.

[46] Dong, Y. F.; Wu, Z. S.; Zheng, S. H.; Wang, X. H.; Qin, J. Q.; Wang, S.; Shi, X. Y.; Bao, X. H. Ti_3C_2 MXene-derived sodium/potassium titanate nanoribbons for high-performance sodium/potassium ion batteries with enhanced capacities. *ACS Nano* **2017**, *11*, 4792–4800.

[47] Zhang, S. L.; Ying, H. J.; Yuan, B.; Hu, R. Z.; Han, W. Q. Partial atomic tin nanocomplex pillared few-layered $Ti_3C_2T_x$ MXenes for superior lithium-ion storage. *Nano-Micro Lett.* **2020**, *12*, 78.

[48] Zhang, J. Z.; Kong, N.; Uzun, S.; Levitt, A.; Seyedin, S.; Lynch, P. A.; Qin, S.; Han, M. K.; Yang, W. R.; Liu, J. Q. et al. Scalable manufacturing of free-standing, strong $Ti_3C_2T_x$ MXene films with outstanding conductivity. *Adv. Mater.* **2020**, *32*, 2001093.

[49] Fang, Y. Z.; Yang, B. W.; He, D. T.; Li, H. P.; Zhu, K.; Wu, L.; Ye, K.; Cheng, K.; Yan, J.; Wang, G. L. et al. Porous and free-standing $Ti_3C_2T_x$-RGO film with ultrahigh gravimetric capacitance for supercapacitors. *Chin. Chem. Lett.* **2020**, *31*, 1004–1008.

[50] Zhang, C. F. Interfacial assembly of two-dimensional MXenes. *J. Energy Chem.* **2021**, *60*, 417–434.

[51] Guan, Y. F.; Jiang, S.; Cong, Y.; Wang, J. P.; Dong, Z. J.; Zhang, Q.; Yuan, G. M.; Li, Y. J.; Li, X. K. A hydrofluoric acid-free synthesis of 2D vanadium carbide (V_2C) MXene for supercapacitor electrodes. *2D Mater.* **2020**, *7*, 025010.

[52] Sarycheva, A.; Gogotsi, Y. Raman spectroscopy analysis of the structure and surface chemistry of $Ti_3C_2T_x$ MXene. *Chem. Mater.* **2020**, *32*, 3480–3488.

[53] Huang, J. M.; Meng, R. J.; Zu, L. H.; Wang, Z. J.; Feng, N.; Yang, Z. Y.; Yu, Y.; Yang, J. H. Sandwich-like $Na_{0.23}TiO_2$ nanobelt/Ti_3C_2 MXene composites from a scalable *in situ* transformation reaction for long-life high-rate lithium/sodium-ion batteries. *Nano Energy* **2018**, *46*, 20–28.

[54] Huang, S. H.; Mochalin, V. N. Hydrolysis of 2D transition-metal carbides (MXenes) in colloidal solutions. *Inorg. Chem.* **2019**, *58*, 1958–1966.

[55] Li, X. L.; Huang, Z. D.; Zhi, C. Y. Environmental stability of MXenes as energy storage materials. *Front. Mater.* **2019**, *6*, 312.

[56] Luo, J. M.; Lu, X.; Matios, E.; Wang, C. L.; Wang, H.; Zhang, Y. W.; Hu, X. F.; Li, W. Y. Tunable MXene-derived 1D/2D hybrid nanoarchitectures as a stable matrix for dendrite-free and ultrahigh capacity sodium metal anode. *Nano Lett.* **2020**, *20*, 7700–7708.

[57] Lee, K.; Yoo, D. Large-area sodium titanate nanorods formed on titanium surface via NaOH alkali treatment. *Arch. Metall. Mater.* **2015**, *60*, 1371–1374.

[58] Yin, L. J.; Li, Y. T.; Yao, X. C.; Wang, Y. Z.; Jia, L.; Liu, Q. M.; Li, J. S.; Li, Y. L.; He, D. Y. MXenes for solar cells. *Nano-Micro Lett.* **2021**, *13*, 78.

[59] Lim, K. R. G.; Handoko, A. D.; Nemani, S. K.; Wyatt, B.; Jiang, H. Y.; Tang, J. W.; Anasori, B.; Seh, Z. W. Rational design of two-dimensional transition metal carbide/nitride (MXene) hybrids and nanocomposites for catalytic energy storage and conversion. *ACS Nano* **2020**, *14*, 10834–10864.

[60] Yuan, W. Y.; Cheng, L. F.; An, Y. R.; Wu, H.; Yao, N.; Fan, X. L.; Guo, X. H. MXene nanofibers as highly active catalysts for hydrogen evolution reaction. *ACS Sustain. Chem. Eng.* **2018**, *6*, 8976–8982.

[61] Pang, S. Y.; Io, W. F.; Wong, L. W.; Zhao, J.; Hao, J. H. Efficient energy conversion and storage based on robust fluoride-free self-assembled 1D niobium carbide in 3D nanowire network. *Adv. Sci.* **2020**, *7*, 1903680.

[62] He, X.; Jin, S.; Miao, L. C.; Cai, Y. C.; Hou, Y. P.; Li, H. X.; Zhang, K.; Yan, Z. H.; Chen, J. A 3D hydroxylated MXene/carbon nanotubes composite as a scaffold for dendrite-free sodium-metal electrodes. *Angew. Chem., Int. Ed.* **2020**, *59*, 16705–16711.

[63] Dong, Y. F.; Zheng, S. H.; Qin, J. Q.; Zhao, X. J.; Shi, H. D.; Wang, X. H.; Chen, J.; Wu, Z. S. All-MXene-based integrated electrode constructed by Ti_3C_2 nanoribbon framework host and nanosheet interlayer for high-energy-density Li-S batteries. *ACS Nano* **2018**, *12*, 2381–2388.

[64] Lian, P. C.; Dong, Y. F.; Wu, Z. S.; Zheng, S. H.; Wang, X. H.; Wang, S.; Sun, C. L.; Qin, J. Q.; Shi, X. Y.; Bao, X. H. Alkalized Ti_3C_2 MXene nanoribbons with expanded interlayer spacing for high-capacity sodium and potassium ion batteries. *Nano Energy* **2017**, *40*, 1–8.

[65] Zheng, S. H.; Ma, J. X.; Fang, K. X.; Li, S. W.; Qin, J. Q.; Li, Y. G.; Wang, J. M.; Zhang, L. Z.; Zhou, F.; Liu, F. Y. et al. High-voltage

potassium ion micro-supercapacitors with extraordinary volumetric energy density for wearable pressure sensor system. *Adv. Energy Mater.* **2021**, *11*, 2003835.

[66] Zhong, W.; Tao, M. L.; Tang, W. W.; Gao, W.; Yang, T. T.; Zhang, Y. Q.; Zhan, R. M.; Bao, S. J.; Xu, M. W. MXene-derivative pompon-like $Na_2Ti_3O_7$@C anode material for advanced sodium ion batteries. *Chem. Eng. J.* **2019**, *378*, 122209.

[67] Ganeshan, K.; Shin, Y. K.; Osti, N. C.; Sun, Y. Y. L.; Prenger, K.; Naguib, M.; Tyagi, M.; Mamontov, E.; Jiang, D. E.; van Duin, A. C. T. Structure and dynamics of aqueous electrolytes confined in 2D-TiO_2/$Ti_3C_2T_2$ MXene heterostructures. *ACS Appl. Mater. Interfaces* **2020**, *12*, 58378–58389.

[68] Zhu, Q. Z.; Li, J. P.; Simon, P.; Xu, B. Two-dimensional MXenes for electrochemical capacitor applications: Progress, challenges and perspectives. *Energy Storage Mater.* **2021**, *35*, 630–660.

[69] Li, N.; Jiang, Y.; Zhou, C. H.; Xiao, Y.; Meng, B.; Wang, Z. Y.; Huang, D. Z.; Xing, C. Y.; Peng, Z. C. High-performance humidity sensor based on urchin-like composite of Ti_3C_2 MXene-derived TiO_2 nanowires. *ACS Appl. Mater. Interfaces* **2019**, *11*, 38116–38125.

[70] Zhang, W. L.; Wei, W.; Liu, W.; Guan, T.; Tian, Y.; Zeng, H. B. Engineering the morphology of TiO_2/carbon hybrids via oxidized $Ti_3C_2T_x$ MXene and associated electrorheological activities. *Chem. Eng. J.* **2019**, *378*, 122170.